On Channel Estimation and Memory Inference in MIMO Wireless Systems

by

Maryam Maryam

A Thesis submitted to The Faculty of Graduate Studies of

The University of Manitoba

in partial fulfillment of the requirements for the degree of

Master of Science

Department of Electrical and Computer Engineering

University of Manitoba

Winnipeg

August 2025

The more I learn, the more I realize how much I don't know.

Albert Einstein

Abstract

The design of robust channel estimation algorithms is essential to meet the increasing demands of next-generation wireless systems. Massive multiple-input multiple-output (MIMO) and ultra-dense antenna deployments present new opportunities for spatial multiplexing and spectral efficiency, but they also introduce challenges that are often overlooked in conventional estimation frameworks. One such challenge is the presence of mutual coupling (MC) among closely spaced antenna elements, which degrades channel state information (CSI) accuracy if not modeled properly. In the first part of this thesis, we address this issue by proposing a physically consistent Kalman filtering framework that accounts for MC effects in compact MIMO arrays through impedance-aware modeling. By embedding coupling transformations into the channel observation model, our method enables recursive tracking of the wireless channel while accurately reflecting the mutual coupling behavior of the antenna array. Simulation results demonstrate significant performance gains over conventional least squares and LMMSE estimators, particularly under strong spatial correlation and compact array configurations.

Building on the spatial-domain improvements in the first part of thesis, we next address the temporal behavior of the channel. Even with MC-aware estimation, pilot-based updates can be costly in fast-changing or resource-limited settings. Instead of estimating the full CSI at every step, we investigate whether the channel's memory and its stability over time can be inferred directly from received signal sequences to guide smarter update decisions. While most estimation algorithms assume quasi-static or memoryless fading, realistic wireless environments exhibit time correlation that can be exploited for prediction and adaptation. We leverage Dynamic Mode Decomposition (DMD) to analyze the evolution of the channel state information (CSI) over time.

By processing sequences of received signals, DMD identifies dominant temporal modes whose spectral properties reveal channel's memory structure. We also compare DMD with principal component analysis (PCA), which processes data statically and captures only dominant variations, whereas DMD uncovers temporal patterns within a dynamical system. Simulation results demonstrate that, unlike PCA, the spectrum of the DMD operator effectively captures the channel memory.

Together, these two contributions form a comprehensive estimation framework that integrates physical modeling with data-driven inference. The results presented in this thesis highlight the importance of accounting for both spatial and temporal effects in wireless channel estimation and point toward more resilient and adaptive communication strategies for 6G and beyond.

Keywords: MIMO, Channel Estimation, Kalman Filtering, Mutual Coupling, Impedance Modeling, Dynamic Mode Decomposition (DMD), Channel Memory, Wireless Communications, 6G

Acknowledgement

I would like to sincerely thank my supervisor, Professor Ekram Hossain, for his continuous guidance, support, and encouragement throughout my graduate studies. His advice and insights have been incredibly valuable at every stage of this work.

A special thanks to Mohamed Akrout for his support, collaboration, and many useful discussions during this journey. His input has played an important role in shaping the direction of this thesis.

I am also thankful to Professor Amine Mezghani for his helpful feedback and technical guidance during this research.

Lastly, I am deeply grateful to my family for always believing in me and to my friends for being there during all the high and low. Your support has meant the world.

Table of Contents

List of Figures

List of Tables

List of Abbreviations

3G	Third Generation (Wireless Communication)
5G	Fifth Generation
6G	Sixth Generation
AR	Autoregressive
AWGN	Additive White Gaussian Noise
BPSK	Binary Phase Shift Keying
CMS	Canonical Minimum Scattering
CSI	Channel State Information
DARE	Discrete Algebraic Riccati Equation
DMD	Dynamic Mode Decomposition
EKF	Extended Kalman Filter
IMM	Interacting Multiple Model
IRS	Intelligent Reflective Surface
KF	Kalman Filter
KVL	Kirchhoff's Voltage Law
LMMSE	Linear Minimum Mean Square Error
LS	Least Squares
MC	Mutual Coupling
MIMO	Multiple Input Multiple Output

ML	Maximum Likelihood
MMSE	Minimum Mean Square Error
mmWave	Millimeter Wave
NMSE	Normalized Mean Square Error
OFDM	Orthogonal Frequency Division Multiplexing
PCA	Principal Component Analysis
PDF	Probability Density Function
QAM	Quadrature Amplitude Modulation
SNR	Signal-to-Noise Ratio
SVD	Singular Value Decomposition
THz	Terahertz
UAV	Unmanned Aerial Vehicle
UWB	Ultra-Wideband
V2X	Vehicle-to-Everything

Chapter 1

Introduction

1.1 Overview

1.1.1 Evolution of Wireless Communication

The evolution of wireless networks from third-generation (3G) to sixth-generation (6G) era has been marked by a dramatic transformation in data demand, user density, and latency constraints. With the deployment of 5G, features such as ultra-low latency, high device density, and elevated data rates have become standard, enabling a range of emerging applications including autonomous mobility [1], remote healthcare [2], and smart city infrastructure [3]. The deployment of massive MIMO systems promises significant improvements in spectral efficiency and connectivity for next-generation wireless networks. Massive MIMO has already emerged as a key enabler for 5G, offering high spectral efficiency and connectivity by employing large antenna arrays with spatial multiplexing [4].

To meet these increasing demands, researchers have turned to advanced technologies including millimeter-wave (mmWave) and sub-terahertz communication, intelligent reflective surfaces (IRS), and massive MIMO. These higher-frequency bands offer greater bandwidths but also introduce challenges such as severe signal attenuation and limited coverage [5]. Among these technologies, massive MIMO has become a cornerstone of 5G and a key enabler for 6G, leveraging large antenna arrays to support spatial multiplexing, enhance spectral efficiency, and enable directional beamforming [6, 7].

However, as massive MIMO scales up—especially in dense deployments—new physical-layer challenges arise, most notably mutual coupling between closely spaced antenna elements. These effects distort the spatial structure of the received signal and degrade channel state information (CSI) quality, motivating the need for physically grounded channel models and estimation frameworks that can accurately account for such hardware impairments [8].

1.1.2 Massive MIMO and Physical Layer Challenges

Fundamentals of Massive MIMO

Massive MIMO achieves its performance gains by increasing the number of antenna elements, enabling simultaneous communication with multiple users through spatial multiplexing. This architecture significantly enhances spectral efficiency, reliability, and network capacity. To meet the extreme data rate and latency demands of future wireless systems, massive MIMO must also operate effectively over wide bandwidths, often in challenging high-frequency regimes such as mmWave and THz [4, 7]. These frequencies introduce new propagation constraints and amplify hardware non-idealities, making accurate channel modeling and estimation even more critical in practical deployments.

Challenges of Mutual Coupling in Realistic Massive MIMO Deployments

One of the most prominent physical-layer impairments in this context is *mutual coupling* (MC), which arises due to near-field interactions among closely spaced antenna elements. As array apertures become increasingly dense to fit large numbers of antennas within constrained form factors, the assumption of ideal, isolated elements becomes untenable. MC not only alters the radiation patterns of the individual elements but also significantly distorts the effective spatial channel perceived by the receiver.

The presence of mutual coupling in dense antenna arrays has long been recognized in electromagnetic theory. Foundational works by Chu [9] and Harrington [10] established the performance limits of electrically small antennas, showing that impedance bandwidth and radiation efficiency are fundamentally constrained by element size and spacing. In the context of massive MIMO, these constraints manifest as spatial correlation and signal distortion that cannot be captured by simplistic channel models.

[11] presented an early and rigorous analytical treatment of mutual coupling effects in broadband MIMO arrays, showing how coupling transforms orthogonal spatial modes into spectrally distinct eigenmodes—thereby impacting the array's spatial degrees of freedom. Further contributions by [12] proposed a circuit-theoretic framework for physically consistent MIMO channel modeling, rooted in impedance network theory. [13] also developed impedance bandwidth-Q bounds for coupled antenna systems, offering a physically grounded methodology to assess array limitations.

Hardware-based decoupling techniques such as coupled line resonators (CLR), laminated resonators (LR), and defected ground structures (DGS) have been explored in works like [14], aiming to mitigate MC through structural design. However, these methods are often expensive, inflexible, or difficult to scale in dynamic scenarios.

Recent studies have revisited MC modeling from a system-level perspective. In [15], the authors propose a compact and physically consistent channel model, demonstrating that MC—if modeled accurately—can in fact be exploited to improve spectral efficiency and bandwidth. This highlights the dual nature of coupling: while often viewed as a detrimental effect, it can become an enabler if treated rigorously.

Need for Physically Consistent Estimation

To address these challenges, we propose a Kalman filtering-based estimation framework that integrates analytical impedance models into the channel observation process. The core idea is to describe both self and mutual interactions among antenna elements using impedance matrices, and to use this representation to transform the received signal into a physically accurate domain. This approach enables the derivation of coupling-aware Kalman filtering recursions that reflect the actual signal distortions introduced by dense array topologies.

Kalman filtering has been widely adopted for channel estimation and tracking in time-varying wireless environments [16, 17]. Its recursive nature allows for real-time tracking of fading channels, especially under linear Gaussian assumptions. Extensions to OFDM and MIMO-OFDM systems include EKF-based designs [18], joint detection-estimation approaches [19], and recent tensor-based learning methods [20].

Adaptive variants like the Interacting Multiple Model (IMM) Kalman filter have also been applied to ultra-wideband (UWB) systems [21], demonstrating robustness to fast channel variations and mobility. More recently, multi-stage Kalman filters have been proposed for sparse channel tracking [22], while robust IMM frameworks have been evaluated in high-mobility scenarios [23]. In hardware-aware applications, [24] extended Kalman estimation to RIS-aided channels under MC.

Despite this progress, few works have integrated full electromagnetic coupling models with Kalman filtering for physically consistent channel tracking in wideband MIMO. In this work, we build upon the impedance-aware modeling framework of [15] and extend it by embedding the coupling structure into a recursive Kalman filtering pipeline for dynamic channel tracking.

By grounding the estimation process in physical system behavior, this work enhances channel tracking accuracy and opens new directions for hardware-aware signal processing architectures in tightly packed MIMO systems.

1.1.3 Importance of Channel State Information

Why Accurate CSI Matters

Accurate channel state information (CSI) is essential for the performance of massive MIMO systems. Beamforming, spatial multiplexing, user scheduling, and interference mitigation all rely on timely and accurate channel estimates. In idealized models, CSI is typically obtained under the assumption that antennas are uncorrelated and behave as independent radiators. However, MC violates this assumption, leading to CSI that poorly reflects the actual propagation environment.

Mutual coupling introduces spatial distortion in dense antenna arrays, altering the radiation and reception patterns of the elements, leading to distorted channel estimates that no longer accurately represents the true propagation environment. These inaccuracies degrade the performance of critical downstream processes, like beamforming, demodulation, and link adaptation. Without a physically consistent framework, estimation errors accumulate, degrading the performance of all downstream processes, including demodulation, decoding, and link adaptation.

While physically consistent CSI estimation is essential for reliable MIMO operation, another underexplored but critical dimension is the temporal structure of the wireless channel itself. In dynamic environments such as vehicle-to-everything (V2X) or UAV-based networks, the wireless channel exhibits temporal correlation, also referred to as channel memory, which can be leveraged to improve tracking and prediction performance [25–27].

Overview of Estimation Techniques

Traditional estimators such as LS, ML, and MMSE are typically designed under quasi-static or memoryless assumptions [28–30]. Although autoregressive (AR) models and Kalman filters have been employed to incorporate temporal memory [31, 32], these methods often rely on strong assumptions like stationarity and require dense pilot usage.

Kalman Filtering in Wireless Systems

Kalman filtering provides a principled approach to recursively estimate the time-varying wireless channel. It models the channel evolution as a Gauss–Markov process and uses a measurement model to update the estimate with new observations. The recursive nature of the filter enables real-time tracking and adaptation, making it particularly useful in mobile and fast-fading conditions.

In the context of MIMO and OFDM systems, a wide range of Kalman-based techniques have been explored, including QRD-based Kalman filters [19], multi-stage Kalman tracking [18], and interacting multiple model (IMM) filters designed to handle dynamic mobility conditions [21, 23]. However, a key limitation across most of this literature is the assumption of ideal or decoupled antenna arrays.

Our work builds on these foundations but explicitly incorporates mutual coupling effects through a physically consistent system model. By embedding impedance-aware transformations into the observation process, the proposed Kalman filter achieves improved estimation fidelity, especially in dense and realistic deployments.

1.1.4 Beyond Estimation: Understanding Channel Memory

Quasi-Static Assumptions in Traditional Estimators

While physically consistent CSI estimation remains crucial for reliable MIMO operation, an equally critical but often overlooked dimension is the temporal correlation structure of the wireless channel—commonly referred to as channel memory. In high-mobility environments such as vehicle-to-everything (V2X) networks, rapidly changing propagation conditions introduce strong temporal dependencies in the channel that, if exploited correctly, can significantly improve prediction and scheduling performance [25, 26].

Conventional estimators like least-squares (LS), maximum-likelihood (ML), and minimum mean square error (MMSE) often assume quasi-static or memoryless channels, limiting their adaptability to fast-fading conditions [29,30,33]. Although autoregressive (AR) models have been used for modeling channel memory in time-correlated fading environments [31, 32, 34], their effectiveness is hampered in highly dynamic scenarios due to inherent assumptions of linearity and stationarity.

In such scenarios, traditional pilot-based and semi-blind techniques also introduce considerable overhead and can fail to adapt effectively, especially when the channel coherence time is short. These limitations have motivated the development of data-driven methods that leverage observed signal dynamics over time to infer channel memory. [35–37].

Dynamic Mode Decomposition

Dynamic Mode Decomposition (DMD) is a data-driven technique used to analyze complex dynamical systems [38]. DMD was initially developed for analysing fluid dynamics but has also gained more prominence in fields such as neuroscience, biology and wireless communication [39] [40]. The DMD advantage lies in its ability to extract spatiotemporal patterns from time-series data. It also does not require any prior knowledge of the underlying physical environment. This makes it ideal for environments where models are not available or they are complex. By linearly approximating the temporal evolution of dynamical systems, DMD identifies the eigenvalues and eigenmodes describing the spatial and temporal dynamics of the system at hand so as to identify and predict its future behavior. Unlike traditional methods such as PCA and SVD which focus on identifying static patterns, DMD captures both the spatial and temporal dynamics of the system, allowing for more accurate characterization of dynamic behaviors.

Channel Memory Inference via Dynamic Mode Decomposition

We propose a data-driven methodology to estimate the channel memory by leveraging the DMD technique. By capturing the temporal evolution of received signal sequences, DMD uncovers dynamic modes whose eigenvalues reflect the channel's underlying memory characteristics. This method eliminates the need for pilot signals and offers a low-complexity, model-free approach suitable for high-mobility environments.

In our work, we tailor the DMD method to wireless communication by applying it to received signal snapshots over multiple time blocks.The DMD algorithm approximates the Koopman operator via singular value decomposition (SVD), whose eigenvalues encode the temporal correlation structure of the channel. Unlike PCA and SVD, which capture only spatial or static patterns, DMD reveals dynamic channel behavior, enabling discrimination between low and high memory regimes using the magnitude of the eigenvalues alone. To the best of our knowledge, this is the first attempt to leverage DMD in the context of wireless communication for memory inference. Our results demonstrate its potential as a powerful tool for channel-aware scheduling and energy-efficient transmission in next-generation mobile networks.

1.1.5 Core Challenges

Despite the growing maturity of massive MIMO technology, a number of key physical phenomena remain inadequately addressed in most practical channel estimation frameworks. One such phenomenon is mutual coupling (MC)—a consequence of electromagnetic interactions between antenna elements placed in close proximity. While MC has long been acknowledged in antenna theory, it has largely been neglected in channel estimation algorithms.

Most classical estimation methods treat the wireless channel as either uncorrelated across antennas or affected only by large-scale propagation-induced correlation. This modeling oversimplification fails to capture the self- and mutual-impedance effects intrinsic to compact antenna arrays. Traditional narrowband assumptions—where the inter-element spacing is large enough to suppress coupling and the channel is modeled as flat across frequency—no longer hold in dense, wideband systems, particularly those operating in mmWave and THz bands [9, 11, 13]. Furthermore, while Kalman filtering and its variants have demonstrated success in recursively tracking time-varying wireless channels, they assume idealized observation models and do not embed physically consistent coupling-aware formulations. Even advanced approaches such as IMM filters for mobility adaptation [21, 23] or multi-stage filtering for sparse channels [22] do not resolve this core modeling deficiency.

In parallel, the temporal structure of wireless channels—commonly referred to as channel memory—remains underutilized. While AR models and Kalman filters can partially exploit temporal correlation, they typically rely on assumptions such as stationary or full pilot availability, which limit their robustness in high-mobility scenarios. Moreover, these techniques require explicit modeling of the channel dynamics, which may not generalize well in non-stationary environments.

There is growing interest in using model-free approaches to extract temporal characteristics, such as channel memory, directly from signal observations. However, very little work has been done to quantify memory levels from a dynamical systems perspective. In particular, no existing study has systematically used Dynamic Mode Decomposition (DMD) to uncover channel memory based solely on signal evolution, without relying on pilot-based supervision.

The two key research gaps addressed in this thesis are:

- The lack of a physically grounded channel estimation approach that incorporates mutual coupling effects through impedance-aware modeling.
- The absence of model-free techniques for quantifying wireless channel memory directly from observed signal dynamics.

1.1.6 Motivation

The challenges identified above, the neglect of mutual coupling in estimation frameworks and the lack of model-free techniques for quantifying channel memory—highlight a critical need for estimation strategies that are both physically accurate and dynamically adaptive.

Rather than viewing mutual coupling as a nuisance to be mitigated, recent work has shown that it can be modeled meaningfully to enhance estimation fidelity in compact arrays [15]. This opens the door to physically grounded approaches that respect the underlying electromagnetic structure of the antenna system, particularly in the wideband and mmWave regimes.

Simultaneously, the dynamic nature of wireless environments calls for inference tools that can adapt to fast-changing conditions without strong assumptions about stationarity, pilot availability, or system structure. Dynamic Mode Decomposition (DMD) presents a compelling alternative: it captures the temporal evolution of signals through spectral analysis of time-series data, allowing the memory of the channel to be inferred directly from observations without relying on predefined models [40].

Motivated by these challenges, this thesis proposes an approach that seeks to advance both physical realism and data-driven adaptability in wireless channel estimation. First, we develop a Kalman filtering framework that explicitly incorporates mutual coupling through impedance-aware modeling. This enables recursive channel tracking that respects the electromagnetic structure of the antenna array. Second, we introduce a Dynamic Mode Decomposition (DMD)-based technique to infer channel memory directly from observed signal sequences, without requiring pilot supervision or prior statistical assumptions.

1.1.7 Contributions

This thesis presents two distinct contributions to the field of wireless channel estimation. The first part of this thesis proposes a Kalman filtering-based channel tracking framework that accounts for mutual coupling (MC) among closely spaced antennas. By embedding these electromagnetic interactions into the channel model and designing a customized Kalman filtering algorithm, the proposed method enables more accurate and physically consistent tracking of MIMO channels. To evaluate the proposed method, extensive simulations are conducted under a variety of SNR conditions, antenna spacings, and temporal correlation regimes. The MC-aware Kalman filter is benchmarked against conventional least squares (LS) and linear MMSE (LMMSE) estimators, showing clear performance gains in both compact and correlated scenarios.

The second part introduces a data-driven method for quantifying wireless channel memory using Dynamic Mode Decomposition (DMD). Unlike model-based techniques that require prior assumptions or pilot signals, this method extracts temporal dynamics directly from sequences of received signals. The proposed approach is tested across a range of noise conditions and channel scenarios, demonstrating its ability to identify underlying memory characteristics and outperform traditional techniques like PCA and SVD in capturing temporal behavior. Simulations are conducted across various SNR levels, noise models (Gaussian and sparse), and temporal correlation regimes. Our results demonstrate that DMD captures dynamic behavior more effectively than traditional techniques like PCA and SVD, which fail to encode temporal evolution. The method operates in a fully unsupervised fashion and requires no knowledge of pilot structure or channel statistics.

1.2 Thesis Organization

This thesis is organized into four chapters, each addressing a core contribution to the advancement of channel estimation techniques in wireless MIMO systems. Chapter 1 provides an introduction to the research, highlighting the motivation, background, and the two main challenges addressed in this work. It outlines the scope, objectives, and contributions of the thesis. Chapter 2 presents a physically consistent channel estimation framework that explicitly accounts for mutual coupling (MC) in MIMO systems. A coupling-aware channel model is developed using impedance matrices, and a Kalman filtering algorithm is designed to operate on this model. Chapter 3 introduces a data-driven methodology for estimating wireless channel memory using Dynamic Mode Decomposition (DMD). The method is tested under various noise models and mobility conditions, showing its effectiveness relative to traditional approaches such as PCA and SVD.Chapter 4 concludes the thesis by summarizing the key contributions and discussing potential future directions.

Chapter 2

Mutual Coupling-Aware MIMO Channel Estimation

2.1 Overview

In this chapter, we present a physically grounded channel estimation framework that incorporates the effects of mutual coupling between antenna elements in MIMO systems. As antenna arrays become more compact and operate over wider bandwidths, the interaction between closely spaced antennas—known as mutual coupling—can no longer be ignored. These effects distort the received signals in ways that standard estimation methods fail to capture, especially when relying on narrowband assumptions.

The main idea in this chapter is to build a model that reflects the actual behavior of the antenna system by using impedance matrices to represent the coupling between elements. This model is then integrated into a recursive estimation approach based on Kalman filtering, enabling the system to track the wireless channel over time while accounting for the coupling-induced distortion.

To develop this framework, we begin by modeling the antenna array using impedance matrices that characterize both self and mutual interactions. These matrices are used to define a transformation that captures how mutual coupling alters the spatial signature of the received signal. Rather than ignoring these effects or treating them as noise, this transformation explicitly embeds coupling into the system model, forming a more realistic representation of the observed channel.

This transformation is incorporated into a recursive estimation process using Kalman filtering, where the wireless channel is modeled as a temporally correlated stochastic process. The filtering mechanism leverages the structure of the coupling-aware measurement model and a Gauss–Markov process for channel evolution, allowing the estimator to track the channel dynamics over time. The key contributions of this chapter are as follows:

- Formulation of a mutual coupling-aware channel observation model based on antenna impedance matrices, capturing both self-impedance and mutual coupling effects in the received signal structure.
- Derivation of a vectorized coupling representation that enables efficient incorporation of impedance interactions into the MIMO system.
- Development of a Kalman filtering algorithm that operates on the modified coupling-aware measurement model.
- Quantitative performance comparison between proposed MC-aware Kalman filter estimation and conventional least squares (LS) and linear MMSE (LMMSE) channel estimation techniques.

2.2 System, Channel and Signal Models

2.2.1 System Model

At super-wideband frequencies and with dense antenna arrays, mutual coupling (MC) becomes an inherent characteristic of the physical channel. Unlike conventional models that treat coupling as a detrimental phenomenon to be mitigated, recent studies have demonstrated that when modeled accurately, MC can enhance spectral efficiency and achievable rates, enabling more compact array designs with improved electromagnetic performance. In particular, Mohamed et al. [15] highlighted that incorporating MC-aware channel models leads to physically consistent formulations that align with fundamental electromagnetic constraints. Motivated by these insights, we develop a Kalman filter-based channel tracking framework that explicitly accounts for antenna impedance interactions and time-varying channel dynamics under realistic array configurations.

2.2.2 Antenna Array Configuration

We consider a MIMO system comprising m transmit and n receive antennas, both arranged in a planar array under far-field propagation conditions.

To model inter-element coupling accurately, we define the antenna impedance matrix $\boldsymbol{Z}$ as:

$$\boldsymbol{v} = \boldsymbol{Z}\boldsymbol{i}, \tag{2.1}$$

where $\boldsymbol{v}$ is the vector of voltages at the antenna ports, and $\boldsymbol{i}$ is the vector of input currents.

The matrix $\boldsymbol{Z}$ has the structure:

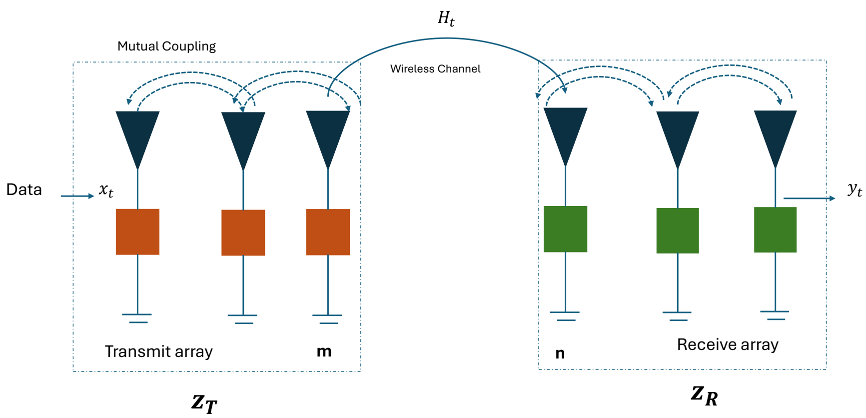

Figure 2.1: Example schematic of the transmit-receive antenna elements configuration with mutual coupling interactions.

$$\boldsymbol{Z} = \begin{bmatrix} Z_{11} & Z_{12} & \cdots & Z_{1N} \\ Z_{21} & Z_{22} & \cdots & Z_{2N} \\ \vdots & \vdots & \ddots & \vdots \\ Z_{N1} & Z_{N2} & \cdots & Z_{NN} \end{bmatrix},$$

In the mutual impedance matrix $\boldsymbol{Z}$, the diagonal terms Z_{ii} correspond to the self-impedance of each antenna, capturing how each element interacts with itself. The off-diagonal terms Z_{ij} for $i \neq j$ represent mutual impedance, quantifying the coupling effect between antenna elements i and j.

2.2.3 Input-Output Relationship

The received signal at time t is modeled as:

$$\boldsymbol{y}_t = \boldsymbol{H}_{\text{phys},t}\boldsymbol{x}_t + \boldsymbol{v}_t, \tag{2.2}$$

where $\boldsymbol{y}_t \in \mathbb{C}^{n\times 1}$ is the received signal vector, $\boldsymbol{x}_t \in \mathbb{C}^{m\times 1}$ is the transmitted pilot vector, and $\boldsymbol{v}_t \sim \mathcal{CN}(0, \sigma_v^2\boldsymbol{I}_n)$ is the additive white Gaussian noise vector.

2.2.4 Impedance-Aware Channel formulation

The physical channel matrix $\boldsymbol{H}_{\text{phys},t}$ incorporating MC effects is expressed as:

$$\boldsymbol{H}_{\text{phys},t} = (\boldsymbol{Z}_R + \boldsymbol{I})^{-1}\boldsymbol{H}_t(\boldsymbol{Z}_T + \boldsymbol{I})^{-1}, \tag{2.3}$$

where $\boldsymbol{Z}_T \in \mathbb{C}^{m\times m}$ and $\boldsymbol{Z}_R \in \mathbb{C}^{n\times n}$ are the transmit and receive array impedance matrices, respectively.

This formulation arises from multiport network theory, where the transformation $(\boldsymbol{Z} + \boldsymbol{I})^{-1}$ accounts for impedance loading and coupling effects shown in Appendix A.

2.2.5 Channel Model

The propagation channel is modeled as

$$\boldsymbol{H}_t = \Re\{\boldsymbol{Z}_R\}^{1/2}\boldsymbol{F}_t\Re\{\boldsymbol{Z}_T\}^{1/2}, \tag{2.4}$$

where $\boldsymbol{F}_t \in \mathbb{C}^{n\times m}$ denotes the fading coefficient matrix at time t. The scaling by $\Re\{\boldsymbol{Z}\}^{1/2}$ ensures the channel model preserves physically realizable power behavior.

2.2.6 Vectorized Channel Representation

For estimation purposes, we vectorize the physical channel as

$$\boldsymbol{h}_{\text{phys},t} = \text{vec}(\boldsymbol{H}_{\text{phys},t}) = \boldsymbol{Z}_{\text{structure}}\boldsymbol{f}_t, \tag{2.5}$$

where $\boldsymbol{f}_t = \text{vec}(\boldsymbol{F}_t) \in \mathbb{C}^{nm\times 1}$ and

$$\boldsymbol{Z}_{\text{structure}} = (\boldsymbol{S}^T\Re\{\boldsymbol{Z}_T\}^{1/2} \otimes \boldsymbol{T}\Re\{\boldsymbol{Z}_R\}^{1/2}). \tag{2.6}$$

Here, $\boldsymbol{S} = (\boldsymbol{Z}_T + \boldsymbol{I})^{-1}$ and $\boldsymbol{T} = (\boldsymbol{Z}_R + \boldsymbol{I})^{-1}$, with $\otimes$ denoting the Kronecker product. This formulation combines transmit and receive coupling transformations into a single linear operator acting on the fading vector.

2.2.7 Temporal Evolution

The time evolution of the fading coefficients follows a first-order Gauss-Markov process:

$$\boldsymbol{f}_t = \sqrt{\alpha}\boldsymbol{f}_{t-1} + \sqrt{1-\alpha}\boldsymbol{w}_t, \tag{2.7}$$

where $\alpha \in [0, 1]$ is the channel memory factor controlling temporal correlation and $\boldsymbol{w}_t \sim \mathcal{CN}(0, \boldsymbol{I})$ is the noise vector representing new independent scattering contributions.

2.2.8 Measurement Model

The observation model at each time slot is given by:

$$\boldsymbol{y}_t = (\boldsymbol{x}_t^T \otimes \boldsymbol{I}_n)\boldsymbol{Z}_{\text{structure}}\boldsymbol{f}_t + \boldsymbol{v}_t. \tag{2.8}$$

Defining $\boldsymbol{B}_t = (\boldsymbol{x}_t^T \otimes \boldsymbol{I}_n)\boldsymbol{Z}_{\text{structure}}$, we can compactly write:

$$\boldsymbol{y}_t = \boldsymbol{B}_t\boldsymbol{f}_t + \boldsymbol{v}_t. \tag{2.9}$$

Here $\boldsymbol{B}_t = (\boldsymbol{x}_t^\top \otimes \boldsymbol{I}_n)\,\boldsymbol{Z}_{\text{structure}}$ is the effective observation matrix incorporating the pilot vector $\boldsymbol{x}_t \in \mathbb{C}^{m\times 1}$ and mutual coupling transformation.

2.2.9 Notation Summary

Table 2.1 summarizes the main symbols used in this chapter.

Table 2.1: Summary of Notation

Symbol	Description
$\boldsymbol{y}_t$	Received signal vector at time t
$\boldsymbol{x}_t$	Transmitted pilot vector at time t
$\boldsymbol{H}_{\text{phys},t}$	Physical channel matrix
$\boldsymbol{Z}_T$, $\boldsymbol{Z}_R$	Transmit and receive impedance matrices
$\boldsymbol{F}_t$	Underlying fading coefficient matrix
$\boldsymbol{f}_t$	Vectorized fading coefficients
$\boldsymbol{Z}_{\text{structure}}$	Impedance transformation matrix
α	Temporal correlation coefficient

2.3 Kalman Filter-Based Channel Estimation

Accurate tracking of time-varying MIMO channels is essential for coherent detection, adaptive beamforming, and robust resource allocation. While static estimators treat each time instant independently, ignoring temporal correlation leads to suboptimal performance, particularly in fast-fading environments. In contrast, Kalman filtering provides an optimal linear recursive estimation framework under Gaussian assumptions by predicting channel evolution based on past dynamics and correcting these predictions using new noisy observations, thus yielding the minimum mean-square error (MMSE) estimate. In this section, we derive the Kalman filtering formualtion for MC-aware channel estimation using the physically consistent system model.

2.3.1 State-Space Formulation

The state evolution and observation models are defined in Eqs. (2.7) and (2.9), respectively, where the channel state $\boldsymbol{f}_t$ evolves as a Gauss–Markov process with temporal correlation coefficient α, and the observation $\boldsymbol{y}_t$ is modeled based on the MC-aware observation matrix $\boldsymbol{B}_t$. Here, $\alpha = 1$ corresponds to a static channel, while $\alpha = 0$ models i.i.d. fast fading.

2.4 Channel Estimation Algorithm

Algorithm 1 MC-Aware Kalman Filter for Channel Tracking

Input: Pilot sequence $\boldsymbol{x}_t$, observation $\boldsymbol{y}_t$, noise covariance $\boldsymbol{R}$, process memory factor α, mutual coupling matrix $\boldsymbol{Z}_{\text{structure}}$

Output: Estimated physical channel $\hat{\boldsymbol{h}}_{\text{phys},t}$ for $t = 1, \ldots, T$

Initialization: Set $\hat{\boldsymbol{f}}_{0|0}$ and error covariance $\boldsymbol{P}_{0|0}$

for $t = 1$ *to* T **do**

Prediction Step:

$\hat{\boldsymbol{f}}_{t|t-1} \leftarrow \sqrt{\alpha}\, \hat{\boldsymbol{f}}_{t-1|t-1}$

$\boldsymbol{P}_{t|t-1} \leftarrow \alpha\, \boldsymbol{P}_{t-1|t-1} + (1-\alpha)\, \boldsymbol{I}$

Kalman Gain Computation:

$\boldsymbol{B}_t \leftarrow (\boldsymbol{x}_t^\top \otimes \boldsymbol{I}_n)\boldsymbol{Z}_{\text{structure}}$

$\boldsymbol{K}_t \leftarrow \boldsymbol{P}_{t|t-1}\boldsymbol{B}_t^H \left(\boldsymbol{B}_t\boldsymbol{P}_{t|t-1}\boldsymbol{B}_t^H + \boldsymbol{R}\right)^{-1}$

Update Step:

$\hat{\boldsymbol{f}}_{t|t} \leftarrow \hat{\boldsymbol{f}}_{t|t-1} + \boldsymbol{K}_t \left(\boldsymbol{y}_t - \boldsymbol{B}_t\hat{\boldsymbol{f}}_{t|t-1}\right)$

$\boldsymbol{P}_{t|t} \leftarrow (\boldsymbol{I} - \boldsymbol{K}_t\boldsymbol{B}_t)\, \boldsymbol{P}_{t|t-1}$

Physical Channel Reconstruction:

$\hat{\boldsymbol{h}}_{\text{phys},t} \leftarrow \boldsymbol{Z}_{\text{structure}}\, \hat{\boldsymbol{f}}_{t|t}$

The Kalman filter algorithm recursively estimates the hidden fading state vector $\boldsymbol{f}_t$

and reconstructs the MC-aware physical channel $\boldsymbol{h}_{\text{phys},t}$ via

$$\hat{\boldsymbol{h}}_{\text{phys},t} = \boldsymbol{Z}_{\text{structure}} \hat{\boldsymbol{f}}_{t|t}. \tag{2.10}$$

Here, $\hat{\boldsymbol{f}}_{t|t}$ denotes the MMSE estimate of the channel coefficients conditioned on all observations up to time t. The inclusion of $\boldsymbol{Z}_{\text{structure}}$ ensures mutual coupling. The Kalman gain $\boldsymbol{K}_t$ adaptively balances confidence between model predictions and noisy measurements, ensuring MMSE optimality at each time step.

On Kalman Filter Stability and Steady-State Behavior In time-invariant linear systems with fixed observation matrix $\boldsymbol{B}$, constant noise statistics, and a stationary channel model (i.e., fixed memory factor α), the Kalman filter error covariance matrix $\boldsymbol{P}_t$ is known to converge to a steady-state solution $\boldsymbol{P}_t$ governed by the Discrete Algebraic Riccati Equation (DARE):

$$\boldsymbol{P} = \alpha\, \boldsymbol{P} - \alpha^2\, \boldsymbol{P}\boldsymbol{B}^{\mathsf{H}} \left(\boldsymbol{B}\alpha\boldsymbol{P}\boldsymbol{B}^{\mathsf{H}} + \boldsymbol{R}\right)^{-1} \boldsymbol{B}\boldsymbol{P} + (1-\alpha)\, \boldsymbol{I}.$$

This convergence is guaranteed under standard assumptions such as the detectability of $(\boldsymbol{B}, \boldsymbol{R})$ and stabilizability of $(\boldsymbol{B}, \boldsymbol{Q}^{1/2})$ [41, 42]. While our channel model explicitly evolves over time via a first-order Gauss–Markov process, the above result provides theoretical assurance.

Tracking performance is evaluated using Normalized Mean Square Error (NMSE) averaged over Monte Carlo trials:

$$\text{NMSE} = \frac{1}{T} \sum_{t=1}^{T} \frac{\|\boldsymbol{h}_{\text{phys},t} - \hat{\boldsymbol{h}}_{\text{phys},t}\|_2^2}{\|\boldsymbol{h}_{\text{phys},t}\|_2^2}. \tag{2.11}$$

2.5 Simulation Setup and Evaluation

To assess the performance of the proposed *impedance-aware* Kalman filtering framework, we conduct extensive Monte Carlo Simulation under various channel and array configurations.

Table 2.2: Simulation Parameters

Parameter	Value(s)
Monte Carlo Runs	1000
Antenna Elements	3^2, 5^2, 10^2
SNR Range (dB)	0 to 50
Pilot Signal Type	BPSK, random Gaussian
Temporal Correlation (α)	0.1, 0.5, 0.9
Coupling Models	MC-aware vs. Non-MC
Antenna Spacing	0.2λ-$\lambda/2$

Channel Model and Pilots The time-varying wireless channel follows a first-order Gauss–Markov process: Pilot signals are drawn from either Gaussian or BPSK distributions. Observations are generated under AWGN

$$\mathrm{SNR} \in \{0, 10, 20, 30, 40, 50\}\ \mathrm{dB}.$$

Each simulation spans $T = 150$ time steps, and results are averaged over 1000 Monte Carlo trials.

2.5.1 Estimation Algorithms and Metrics

Estimators Compared We evaluate and compare the following estimation techniques:

- **Full mutual coupling-aware estimator**: incorporates the complete impedance structure.
- **Mutual coupling Unaware**: neglects off-diagonal coupling terms and hence ignores mutual coupling effects.

Comparative Analysis To evaluate the performance of the proposed Kalman filtering framework, we benchmark against two widely used estimators: the Least Squares (LS) and the Linear Minimum Mean Square Error (LMMSE) methods. The LS estimator is a natural baseline due to its simplicity and model-agnostic nature. It estimates the channel solely based on pilot observations without incorporating prior statistical knowledge or temporal correlation. The LMMSE estimator incorporates second-order channel statistics, yielding better performance than LS in many settings. However, it still lacks temporal recursion and does not adapt to time-varying dynamics.

Performance Metric Channel estimation accuracy is quantified using the Normalized Mean Squared Error (NMSE):

$$\mathrm{NMSE} = \frac{1}{T}\sum_{t=1}^{T}\frac{\|\boldsymbol{h}_t - \widehat{\boldsymbol{h}}_t\|_2^2}{\|\boldsymbol{h}_t\|_2^2}. \tag{2.12}$$

2.5.2 Evaluation Scenarios

We consider multiple evaluation setups to examine behavior under different configurations:

NMSE Performance Across SNR Levels

To assess the impact of array geometry and measurement conditions on estimation performance, we conduct simulations using antenna elements of sizes 3×3, 5×5, and 10×10, under both underdetermined and overdetermined scenarios. For each configuration, we consider inter-element spacings of 0.2λ and 0.5λ, representing densely packed and critically spaced arrays, respectively.

In Fig. 2.2(a), where the antenna spacing is 0.2λ we observe that the NMSE improves with increasing SNR across all correlation coefficients ($\alpha = 0.1, 0.5, 0.9$). However, the gap between MC-aware and MC-unaware performance becomes more visible as the channel becomes more correlated (higher α). This shows that mutual coupling effects become more significant under strong temporal correlation, and MC-aware filtering helps mitigate this degradation effectively. Kalman filter leverages a recursive prediction-update framework that incorporates prior state estimates and channel dynamics. This feature enables the filter to track the slowly varying channel more effectively compared to static estimators.

For instance, at $\alpha = 0.9$ and SNR = 30 dB, the MC-aware method shows nearly 50% lower NMSE compared to the MC-unaware one. This highlights the necessity of incorporating MC models in tightly packed antenna arrays.

In contrast, Fig. 2.2(b), corresponding to a 0.5λ spacing, exhibits a significantly narrower performance gap between MC-aware and MC-unaware estimators. As we increase the spacing between antenna elements, physical interaction between antenna elements reduces. Consequently, the benefit of MC-aware estimation becomes less significant but MC-aware still marginally outperforms the MC-unaware approach.

Compared to the underdetermined case, the overdetermined setting in Fig.(2.3) offers more observations than unknowns, improving Kalman filter resolution and estimation accuracy. Both MC-aware and MC-unaware Kalman filters show improved NMSE performance as SNR increases. The MC-aware estimator continues to outperform the MC-unaware version across all SNR levels and α values shown in Fig. 2.3(a). The performance gap is especially notable for higher correlation ($\alpha = 0.9$), where the benefit of modeling mutual coupling becomes more evident. Additionally, when spacing at 0.5λ shown in Fig. 2.3(b), both MC-aware and MC-unaware Kalman filters achieve nearly identical NMSE across all SNRs and α values. The two curves stay overlapped throughout, indicating that the additional pilot information allows accurate estimation even without modeling mutual coupling. Moreover, the larger antenna spacing weakens coupling effects, further reducing the gap between the two methods.

Following the analysis in Fig.(2.2), similar evaluations are conducted for higher-

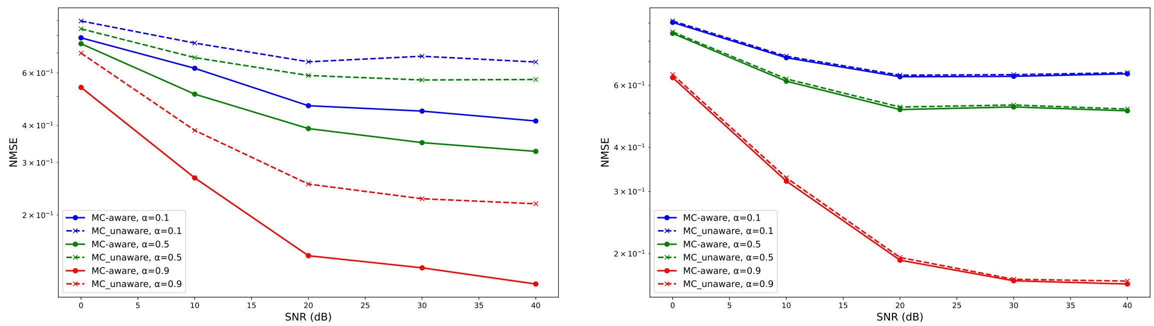

(a) Spacing 0.2λ

(b) Spacing 0.5λ

Figure 2.2: NMSE comparison between MC-aware and MC-unaware Kalman filters for a 3×3 antenna elements using BPSK pilot signals in the underdetermined scenario.

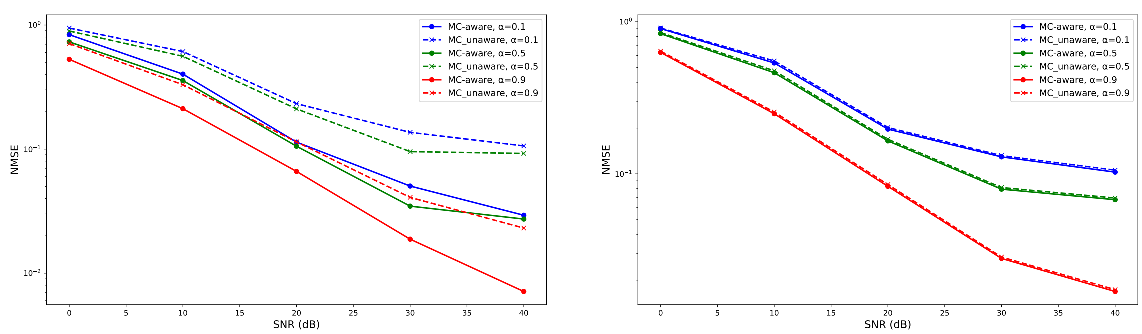

(a) Spacing 0.2λ

(b) Spacing 0.5λ

Figure 2.3: NMSE comparison between MC-aware and MC-unaware Kalman filters for a 3×3 antenna elements using BPSK pilot signals in the overdetermined scenario.

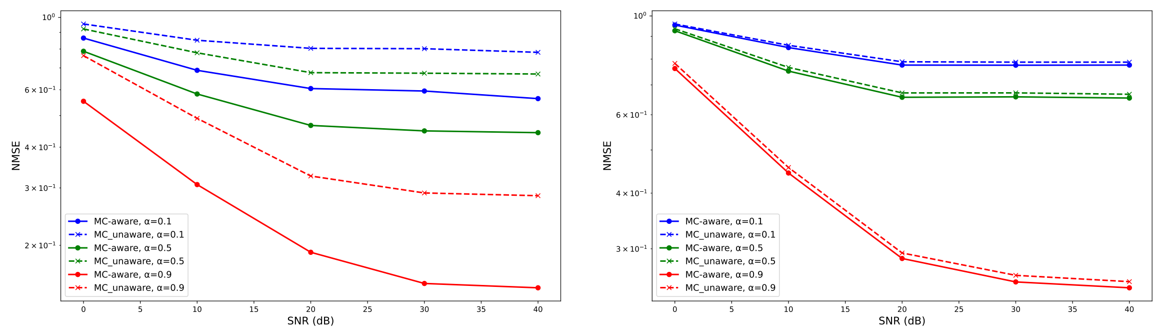

(a) Spacing 0.2λ (b) Spacing 0.5λ

Figure 2.4: NMSE comparison between MC-aware and MC-unaware Kalman filters for a 5×5 antenna elements using BPSK pilot signals in the underdetermined scenario.

dimensional antenna elements, specifically 5×5 and 10×10 configurations as shown in Fig. (2.4) and (2.6). Both underdetermined and overdetermined scenarios are examined using spacings of 0.2λ and 0.5λ for case of 5×5 . As it can be seen that the observed trends remain consistent and MC-aware Kalman filtering maintains superior NMSE performance across all settings compared to its MC-unaware counterpart. As the antenna array size increases, the benefits of incorporating mutual coupling become more pronounced, especially in low-noise (high SNR) regimes. Furthermore, the larger spacing of 0.5λ shown in Figs. 2.4(b),2.5(b) and 2.6(b) continues to slightly enhance estimation accuracy, due to reduced mutual coupling effects. These results collectively reinforce the scalability and robustness of MC-aware filtering approaches in practical massive MIMO systems.

Continuing the analysis, Fig.(2.7) illustrates the NMSE performance of MC-aware and MC-unaware Kalman filters across increasing antenna array sizes under the underdetermined regime, using BPSK pilot signals. As shown in Fig. 2.7(a), for a dense array with spacing 0.2λ, NMSE degrades with array size due to high mutual coupling and due to the growth in the number of unknowns relative to fixed measurement resources. But

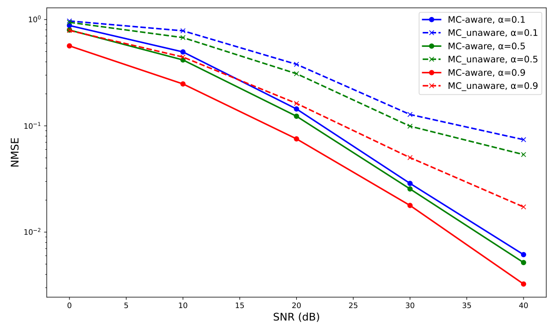

(a) Spacing 0.2λ

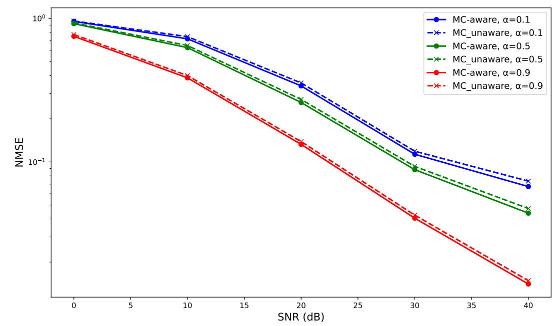

(b) Spacing 0.5λ

Figure 2.5: NMSE comparison between MC-aware and MC-unaware Kalman filters for a 5×5 antenna elements using BPSK pilot signals in the overdetermined scenario.

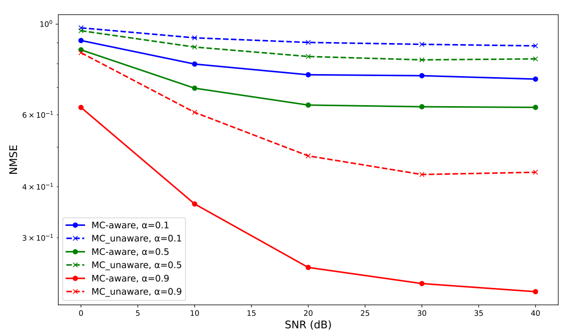

(a) Spacing 0.2λ

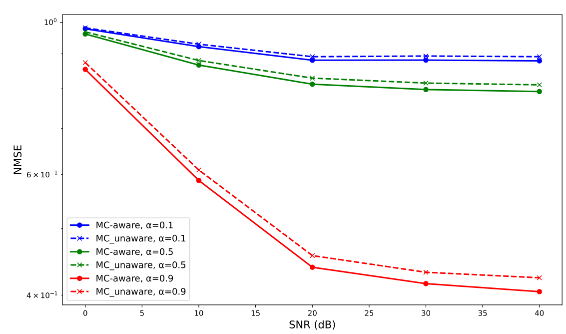

(b) Spacing 0.5λ

Figure 2.6: NMSE comparison between MC-aware and MC-unaware Kalman filters for a 10×10 antenna elements using BPSK pilot signals in the underdetermined scenario.

we can notice that the MC-aware filter still achieves lower NMSE compared to its de-coupled scenario, and this gap increases as we move towards higher channel correlation ($\alpha = 0.9$).

Fig. 2.7(b), shows that spacing 0.5λ, exhibits similar behavior. The MC-aware estimator continues to outperform the MC-unaware version, but the gain is smaller, especially for low correlation ($\alpha = 0.1$). These results confirm that MC-aware filtering remains effective even as the number of antennas increases.

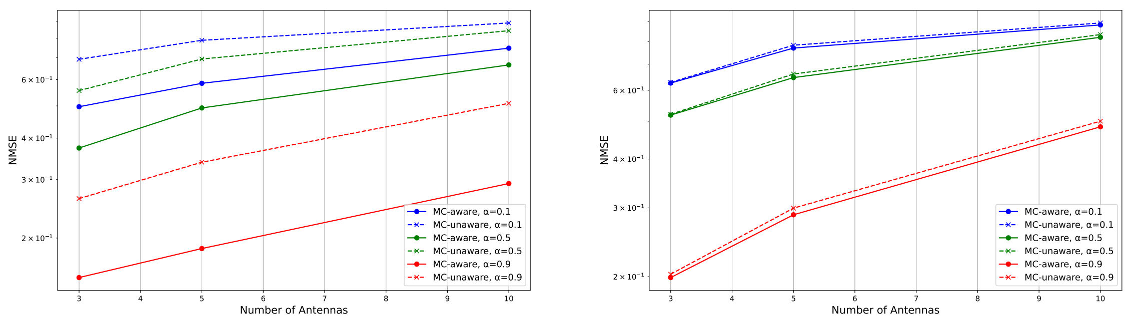

(a) Spacing 0.2λ (b) Spacing 0.5λ

Figure 2.7: NMSE comparison between MC-aware and MC-unaware Kalman filters for varying antenna array sizes.

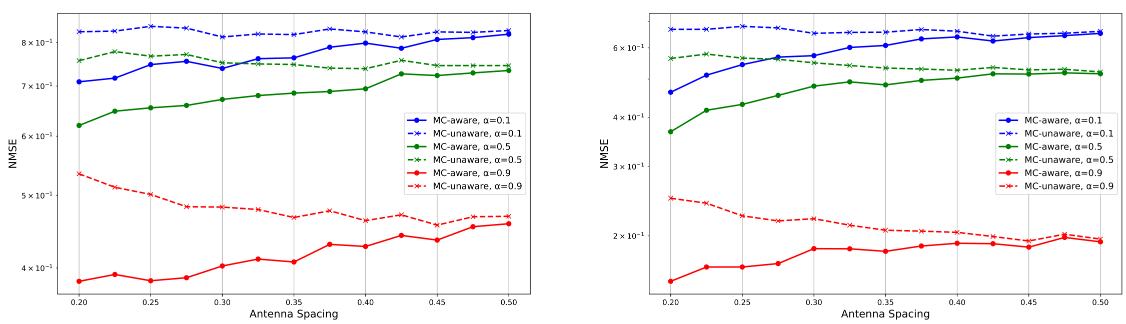

(a) SNR = 5 dB (b) SNR = 20 dB

Figure 2.8: NMSE performance of MC-aware and MC-unaware Kalman filters for a 3×3 antenna elements across varying antenna spacings . Each curve corresponds to a different temporal correlation factor.

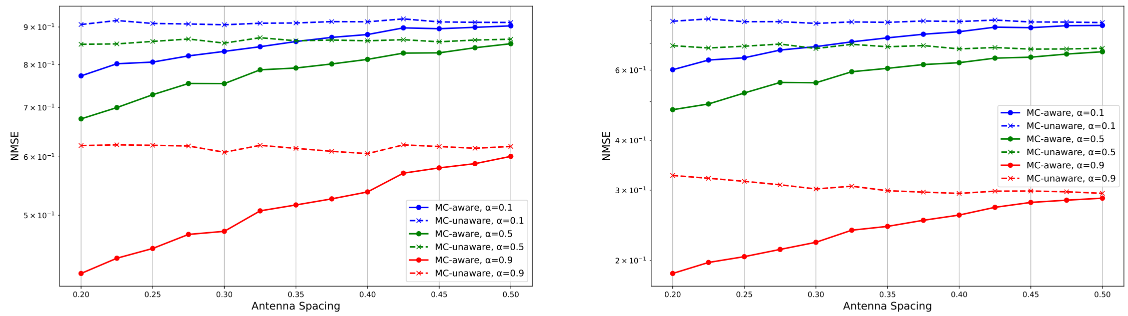

(a) SNR = 5 dB

(b) SNR = 20 dB

Figure 2.9: NMSE performance of MC-aware and MC-unaware Kalman filters for a 5×5 antenna elements across varying antenna spacings.

Figs. (2.8) and (2.9) show the NMSE performance of the MC-aware and MC-unaware Kalman filters for 3×3 and 5×5 antenna arrays across different antenna spacings. As expected, the MC-aware filter consistently achieves lower estimation error, particularly when the temporal correlation is high (e.g., $\alpha = 0.9$). As the spacing increases, the performance of both filters begins to converge, which is intuitive since mutual coupling effects diminish with greater inter-element distance. These results support the effectiveness of the proposed MC-aware framework, especially in compact array configurations where coupling is more pronounced.

Benchmarking Strategy We benchmark the proposed MC-aware Kalman Filter technique against a conventional LMMSE estimator across different temporal correlation by varying α values. Fig. (2.10) shows the results for 3×3 antenna elements under two antenna spacings: 0.2λ and 0.5λ using BPSK pilot signals. We note that Kalman filter takes advantage of the temporal evolution defined in Eq. (2.7), where the channel coefficient $\boldsymbol{f}_t$ follows a first-order Gauss-Markov process with temporal correlation governed by α. As α increases. the Kalman estimator benefits from past channel estimates, and improves the prediction and update over time. This dynamic modeling leads to a reduction in the estimation error, especially for $\alpha = 0.9$, where the NMSE improves,

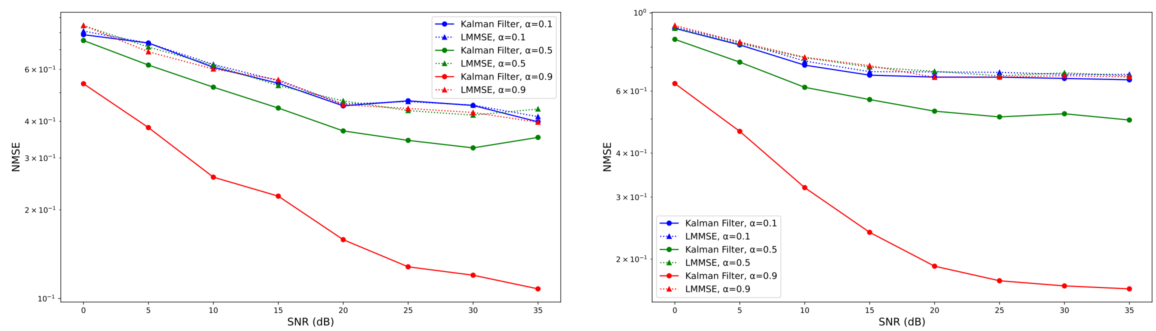

(a) Spacing 0.2λ (b) Spacing 0.5λ

Figure 2.10: Comparison of Kalman filter performance against an LMMSE baseline across different temporal dynamics (α values) for3×3 antenna elements

outperforming the LMMSE in higher SNR regime. On the other hand, the LMMSE estimator treats each time slot as an independent realization of the channel because it operates in a memoryless fashion and estimates solely based on current observation and does not adapt to time-varying dynamics. Consequently, the NMSE performance of LMMSE remains largely invariant with respect to α. As α increases, the performance gap between LMMSE and Kalman filtering becomes increasingly significant, showing the advantage of sequential estimation methods in time-varying channels. Moreover, both spacing cases exhibit similar trends, though the effect of mutual coupling is more visible in tightly packed $0.2\ \lambda$ configuration.

Building upon the performance of the LMMSE estimator, we further compare the proposed Kalman filtering framework with the conventional Least Squares (LS) estimator under varying temporal correlation conditions as shown in Fig.(2.11). The LS estimator, being a static one-shot approach, does not leverage the temporal evolution of the channel and treats each time step independently.

In contrast, the Kalman filter explicitly models the temporal state-space evolution governed by the correlation factor α and exploits this structure recursively over time.

As a result, its NMSE performance consistently outperforms LS, especially at higher α values in Fig. 2.11(a) where channel states evolve slowly and thus benefit more from prediction-based estimation.

In Fig. 2.11(a), under $\alpha = 0.9$ and spacing 0.2λ, the Kalman filter shows improvements over LS across all SNR values. This improvement becomes even more pronounced in Fig. 2.11(b), where spatial correlation effects from critical spacing (0.5λ) are mitigated more effectively by the Kalman recursion. These observations reaffirm the advantage of incorporating temporal dynamics via Kalman filtering, as opposed to memoryless estimation approaches such as LS. From benchmarking against LMMSE and LS we we see that although the LMMSE estimator leverages second-order channel statistics to achieve improved accuracy over LS in various scenarios, it still remains limited by its lack of temporal adaptation. Both LS and LMMSE operate without exploiting the recursive nature of time-varying channels. This comparison further shows the advantages of Kalman filtering, particularly in dynamically evolving and spatially coupled environments where both temporal correlation and mutual coupling significantly impact estimation performance.

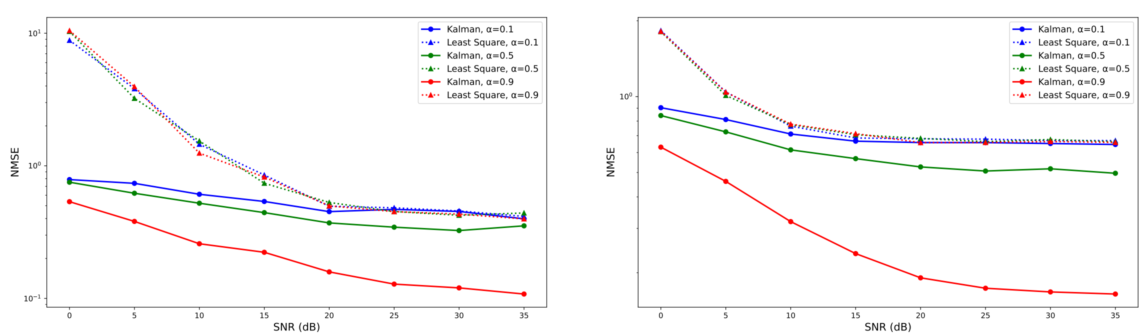

(a) Spacing 0.2λ

(b) Spacing 0.5λ

Figure 2.11: Comparison of Kalman filter performance against an Least Square (LS) baseline across different temporal dynamics (α values)

Conclusion

In this chapter, we proposed a physically consistent Kalman filtering framework for channel estimation in MIMO systems that explicitly accounts for mutual coupling (MC) effects. By incorporating an impedance-aware model, our approach captures the spatial correlation introduced by coupling between antenna elements. This coupling-aware model was integrated into the Kalman filter structure, enabling accurate and recursive tracking of the wireless channel over time. Through simulation results under varying SNR, antenna spacings, and temporal correlation settings, the proposed MC-aware estimator demonstrated superior performance compared to conventional LS and LMMSE benchmarks. These results highlight the importance of incorporating MC effects into the estimation process, especially in compact and correlated MIMO arrays.

Chapter 3

Inferring the Channel Memory from Received Signals Using Dynamic Mode Decomposition

3.1 Problem Overview and Research Contributions

Estimating the memory of wireless fading channels is crucial for developing predictive and adaptive communication strategies, particularly in fast-varying environments such as vehicular networks. Traditional estimation methods rely on predefined statistical models or dense pilot transmissions, both of which may be impractical or inaccurate under non-stationary conditions. To address these limitations, this chapter presents a data-driven approach for channel memory inference based solely on received signal observations.

The method leverages the Dynamic Mode Decomposition (DMD) algorithm to analyze temporal patterns embedded in sequences of received signals. While the theoretical foundations of DMD and its relation to the Koopman operator are discussed in Chapter 1, this chapter focuses on the design and simulation of a practical framework that applies DMD to wireless channel data in order to infer the temporal memory factor. The approach does not require prior knowledge of the channel model, and it operates without pilot symbols, making it suitable for low-latency or bandwidth-constrained scenarios. The main contributions of this chapter are summarized as follows:

- We tailor the DMD method to the estimation of the channel memory for wireless multiple-input multiple-output (MIMO) communication.
- We propose the maximum eigenmode of the DMD operator as a metric to infer the channel memory for a time-slotted wireless system.
- We compare the DMD method with principal component analysis (PCA) and singular value decomposition (SVD) methods. Simulation results show that unlike PCA and SVD, DMD effectively captures the temporal dynamics of channel memory, making it a promising tool for vehicular communication scenarios.

3.2 System Models

Algorithm 2 Dynamic Mode Decomposition (DMD)

Input: Sequence of received signals over B time blocks: $\{\boldsymbol{y}_1, \boldsymbol{y}_2, \ldots, \boldsymbol{y}_B\}$

Output: DMD modes $\boldsymbol{U\Phi}$ and eigenvalues $\boldsymbol{\Lambda}$

1 Construct snapshot matrices:

$\boldsymbol{Y}_{1:B-1} \leftarrow [\boldsymbol{y}_1, \ldots, \boldsymbol{y}_{B-1}]$

$\boldsymbol{Y}_{2:B} \leftarrow [\boldsymbol{y}_2, \ldots, \boldsymbol{y}_B]$

2 Compute singular value decomposition:

$\boldsymbol{Y}_{1:B-1} = \boldsymbol{U\Sigma V}^*$

3 Compute low-rank approximation of Koopman operator:

$\widetilde{\boldsymbol{A}} = \boldsymbol{U}^* \boldsymbol{Y}_{2:B} \boldsymbol{V\Sigma}^{-1}$

4 Compute eigen-decomposition of $\widetilde{\boldsymbol{A}}$:

$\widetilde{\boldsymbol{A}}\boldsymbol{\Phi} = \boldsymbol{\Phi\Lambda}$

DMD is employed in this work as a data-driven approach for capturing the temporal dynamics of the received signal without relying on an explicit model of the channel evolution. This chapter focuses on its application to the problem of channel memory estimation in wireless communication systems.

We first begin by formulating the core data-driven operator approximation procedure underlying DMD and then describe how it can be adapted to capture the temporal dynamics inherent in time-slotted wireless environments. Consider a dataset obtained from T observable states, each corresponding to a single data snapshot $\boldsymbol{y}_t \in \mathbb{R}^M$ for $t \in [1, \ldots, T]$. The observed states can then be stacked to construct the following two matrices:

$$\boldsymbol{Y}_{1:T-1} = \begin{bmatrix} | & | & & | \\ \boldsymbol{y}_1 & \boldsymbol{y}_2 & \cdots & \boldsymbol{y}_{T-1} \\ | & | & & | \end{bmatrix} \in \mathbb{R}^{M\times(T-1)}, \tag{3.1a}$$

$$\boldsymbol{Y}_{2:T} = \begin{bmatrix} | & | & & | \\ \boldsymbol{y}_2 & \boldsymbol{y}_3 & \cdots & \boldsymbol{y}_{T} \\ | & | & & | \end{bmatrix} \in \mathbb{R}^{M\times(T-1)}. \tag{3.1b}$$

Note here how $\boldsymbol{Y}_{2:T}$ is the time-shifted matrix of $\boldsymbol{Y}_{1:T-1}$. The goal of DMD is to find the best approximation of the local linear operator $\boldsymbol{A}$ which satisfies:

$$\boldsymbol{Y}_{2:T} = \boldsymbol{A}\,\boldsymbol{Y}_{1:T-1}. \tag{3.2}$$

Here the matrix $\boldsymbol{A}$ is referred to as the Koopman operator representing the linear operator that captures the ability to predict the state $\boldsymbol{y}_T$ given all previous states for $t \in [1, T-1]$. For high dimensional dynamical systems, direct computation of $\boldsymbol{A}$ can be computationally expensive. Instead, a reduced-order approximation is computed using SVD. The eigenvectors of $\boldsymbol{A}$ are called the DMD modes while the eigenvalues are referred to as the DMD eigenvalues. Each DMD eigenvalue presents the significance of the temporal behavior associated with the corresponding eigenvector. When the dimension of the system M is large, DMD does not directly compute the eigenvectors and eigenvalues but rather approximates them using a low-rank approximation as shown in Algorithm 2.

System Model and Assumptions

We consider a MIMO communication system between N transmit antennas and M receive antennas. This operates under the Gauss-Markov Rayleigh fading process. The time blocks B are used to transmit K symbols. This system model builds upon and extends the framework proposed in [43] and is reproduced with permission from the original authors, with modifications to incorporate an inference framework for estimating channel memory factor using DMD.

For every time-block b, the received signal is given by:

$$\boldsymbol{y}_b = \boldsymbol{H}_b \boldsymbol{x}_b + \boldsymbol{n}_b, \qquad b = 1, \ldots, B. \tag{3.3}$$

In equation (3.3), $\boldsymbol{x}_b \in \mathbb{C}^N$ shows the transmitted symbol vector and $\boldsymbol{n}_b \in \mathbb{C}^M$ is an additive complex white Gaussian noise vector, i.e., $\boldsymbol{n}_b \sim \mathcal{CN}(\mathbf{0}_M, \sigma^2_{\boldsymbol{n}_b} \boldsymbol{I}_M)$. At a given SNR level ρ [dB], the noise variance $\sigma^2_{\boldsymbol{n}_b}$ is defined as:

$$\sigma^2_{\boldsymbol{n}_b} = \boldsymbol{E}\Big[\boldsymbol{H}_b \boldsymbol{x}_b{}^2\Big]\, 10^{-\rho/10}. \tag{3.4}$$

In addition, $\boldsymbol{H}_b$ shows the time-varying Rayleigh fading channel evolving according to the first-order Gauss-Markov model [44]:

$$\boldsymbol{H}_b = \sqrt{\alpha}\, \boldsymbol{H}_{b-1} + \sqrt{1-\alpha}\, \boldsymbol{W}_b, \qquad b = 2, \ldots, B, \tag{3.5}$$

where $\alpha \in [0, 1]$ is the channel memory factor. Moreover, $\boldsymbol{H}_1$ and $\boldsymbol{W}_b$ are drawn from the complex Gaussian distribution $\mathcal{CN}(\mathbf{0}_{NM}, \boldsymbol{I}_{NM})$ and are independent and identically distributed realization. In some scenarios, the noise $\boldsymbol{n}_b$ can also be modeled as sparse noise to account for infrequent but large disturbances. By recursively injecting the expression of $\boldsymbol{H}_{b-1}$ in (3.5) for $b = 1, \ldots, B$, we obtain:

$$\boldsymbol{H}_b = \sqrt{\alpha}^{b-1}\, \boldsymbol{H}_1 + \sqrt{1-\alpha} \sum_{p=2}^{b} \sqrt{\alpha}^{b-p}\, \boldsymbol{W}_p. \tag{3.6}$$

Consequently, the sequence $\{\boldsymbol{H}_b\}_{b=1}^{B}$ in (3.6) constitutes a discrete-time Markov chain that evolves as a random walk, and it starts from the initial channel $\boldsymbol{H}_1$ and scaled by the factor $\sqrt{\alpha}^{,b-1}$ at the b-th block. This Markov chain process captures the stochastic nature of channel aging, which causes notable shifts in the channel distribution. Channel aging arises from the time variation between when the channel is estimated using pilots and when it is subsequently used for signal processing, with this variation driven by user mobility and processing delays [43].

The memory in the channel matrix $\boldsymbol{H}_b$ is controlled by the parameter α, which determines how much of the previous channel state $\boldsymbol{H}_{b-1}$ is retained in the current channel state $\boldsymbol{H}_b$. When α is close to 1, the channel has high memory, meaning it changes slowly over time. Conversely, when α is close to 0, the channel state is largely determined by the new noise matrix $\boldsymbol{W}_b$, and hence exhibits low memory. The induced memory in $\boldsymbol{y}_b$ depends on the channel memory $\boldsymbol{H}_b$. When $\boldsymbol{H}_b$ has a high memory (i.e., α is high), changes in $\boldsymbol{H}_b$ from one block to the next are relatively small, which means that the effect of the channel on the transmitted signal $\boldsymbol{x}_b$ also changes slowly. In other words, $\boldsymbol{y}_b$ indirectly reflects the memory of the channel $\boldsymbol{H}_b$ over successive blocks. This observation justifies why the use of data-driven methods on channels exhibiting a memory level can be inferred solely based on the received signals.

Applying DMD for wireless received signals

For our study, the received vector $\boldsymbol{y}_t$ in (3.3) plays the role of the observable state $\boldsymbol{y}_t$ in (3.1) as reflects all the communication effects induced by the channel and the noise. As a result, we construct snapshot matrices $\boldsymbol{Y}_{1:B-1}$ and $\boldsymbol{Y}_{2:B}$ from sequences of received signals as indicated in (3.1). The key idea of this paper is to leverage the eigenvalues of the DMD approximation of the Koopman operator $\boldsymbol{A}$ to inform about the channel memory of the channel only by processing received signal data. By doing so, DMD tailored to wireless devices offers an important side of channel memory at the cost of low processing complexity.

The correlation between the snapshots of receive signals $\boldsymbol{Y}_{1:B-1}$ and its subsequent $\boldsymbol{Y}_{2:B}$ depends on the channel memory. The induced DMD modes exhibit a higher correlation with the progression from one time-block to the next one and become more significant with larger channel memories as they dictate the dynamic evolution of the channel. Because the eigenvalues of the approximated Koopman operator $\boldsymbol{A}$ quantifies this significance, it becomes apparent why considering the norm of the DMD eigenvalues associated with DMD modes indirectly mirrors the effect of the channel memory. In scenarios where the channel memory factor is variable, DMD can be adapted by dividing the received signal into different time blocks. For instance, using the first half of the received signal vectors, the channel memory can be estimated for the initial time period, and the second half can be used for the subsequent period to ensure that the variable memory is captured dynamically.

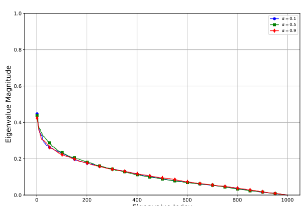

(a) DMD, SNR = −20 dB.

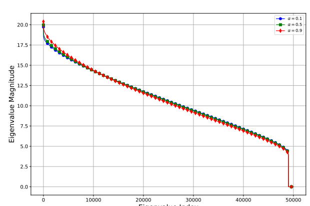

(b) SVD, SNR = −20 dB.

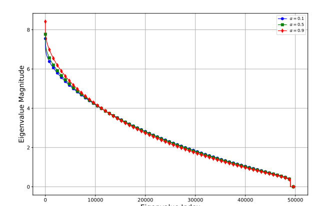

(c) PCA, SNR = −20 dB.

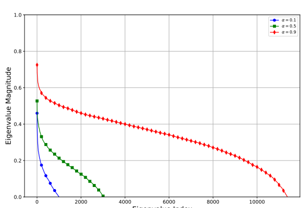

(d) DMD, SNR = 20 dB.

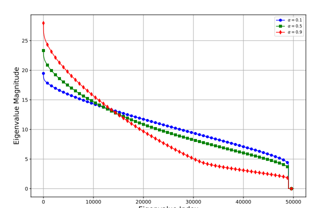

(e) SVD, SNR = 20 dB.

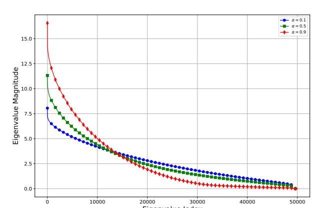

(f) PCA, SNR = 20 dB.

Figure 3.1: Spectrums with Gaussian noise sources for different values of channel memory α: (a,d) DMD at SNR = −20 and 20 dB, (b,e) SVD at SNR = −20 and 20 dB, (c,f) PCA at SNR = −20 and 20 dB.

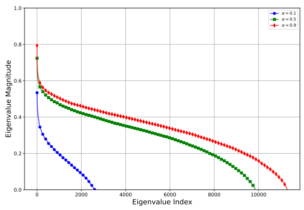

(a) DMD, SNR = -20 dB.

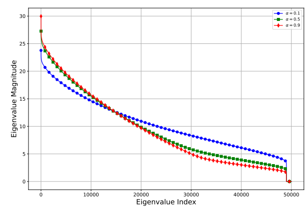

(b) SVD, SNR = -20 dB.

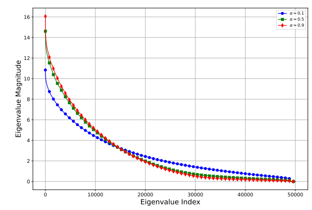

(c) PCA, SNR = -20 dB.

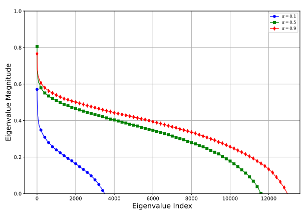

(d) DMD, SNR = 20 dB.

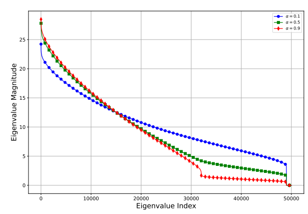

(e) SVD, SNR = 20 dB.

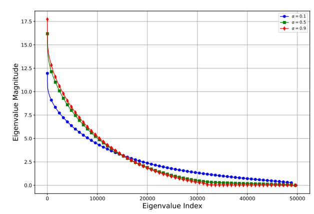

(f) PCA, SNR = 20 dB.

Figure 3.2: Spectrums with sparse noise sources for different values of channel memory α: (a,d) DMD at SNR $= -20$ and 20 dB, (b,e) SVD at SNR $= -20$ and 20 dB, (c,f) PCA at SNR $= -20$ and 20 dB.

3.3 Simulation Results

In this section, we present our simulation results for DMD and PCA using the received model in (3.3). Table 3.1 describes the values of the key parameters.

Each simulation is run for $N_{\mathrm{MC}} = 2000$ Monte-Carlo trials. Moreover, both the measurement equation of the received signal in (3.3) and the channel dynamics' equation in (3.5) are perturbed by noise sources. To explore the effectiveness of DMD, PCA and SVD, we vary the priors on $\boldsymbol{n}_b$ and $\boldsymbol{W}_b$ to be either Gaussian or Bernoulli-sparse with 90% sparsity. We also vary the SNR ρ to study the amplitude of the spectrum of the approximate Koopman operator in DMD, the covariance matrix in PCA and the singular values in SVD. Throughout the simulations, we will call the former the *DMD spectrum* and the latter the *PCA and SVD spectrums*.

Table 3.1: Simulation parameters

Parameter	Description	Value(s)
B	Time-block	50
N	Transmit antennas	32
M	Receive antennas	128
K	Symbol per time-block	1
ρ	SNR in dB	{-20, 0, 20}
α	Memory factor	{0.1, 0.5, 0.9}
$\boldsymbol{x}_b$	Transmitted symbols	BPSK: {-1,1}

We investigate the ability of DMD against PCA and SVD to capture of the channel memory through the analysis of the DMD, PCA and SVD spectrums when $\boldsymbol{n}_b$ and $\boldsymbol{W}_b$ are Gaussian. The DMD spectrums for SNR $= -20\,\mathrm{dB}$ and SNR $= 20\,\mathrm{dB}$ are shown in Figs. 3.1(a) and 3.1(d) while those of PCA and SVD are depicted in Figs. 3.1(c), 3.1(f) and 3.1(b) , 3.1(e). First, we note that at low SNR (e.g., SNR $= -20\,\mathrm{dB}$), all spectrums drop off gradually independently of the memory factor α. Indeed, all plots in Fig. 3.1(a), 3.1(c), and 3.1(b) almost coincide, suggesting that the channel memory estimation is a challenging task under high noise levels. Conversely, Figs. 3.1(d), 3.1(f), and 3.1(e) depict the DMD, SVD and PCA spectrums at high SNR (e.g., SNR $= 20\,\mathrm{dB}$). Fig. 3.1(d) shows how the DMD spectrum widens as the channel memory increases from $\alpha = 0.1$ (in blue) up to $\alpha = 0.9$ (in red). This is because higher channel memory requires a larger number of modes to capture the underlying patterns of the dynamical system according to which the received signals are obtained. In other words, the approximate Koopman operator becomes lower rank as the memory of the channel decreases. The same observation does not hold for the PCA and SVD spectrums shown in Figs. 3.1(f) and 3.1(e), respectively. There, the PCA and SVD spectrums for all channel memories have a heavy tail. Such a result is indeed expected because the PCA analysis focuses on maximal variations and does not explicitly account for the temporal behavior of the system's dynamics. Similarly, the SVD method focuses on the variation in the eigenmode directions. It is interesting however to observe how the PCA and SVD spectrums intersect. At the left of the intersection, the higher the channel memory the larger the PCA and SVD spectrums, while larger spectrums at the right of the intersection correspond to received signals with smaller channel memory. This suggests that the eigenvalues at the left capture the channel component $\sqrt{\alpha}\,\boldsymbol{H}_{b-1}$ in the Gauss-Markov channel dynamics in (3.5), while those at the right are induced by the noise component $\sqrt{1-\alpha}\,\boldsymbol{W}_b$. Clearly, the PCA and SVD spectrums do not enjoy the low-rank structure as the approximate Koopman operator in DMD. In practice, PCA and SVD spectrums have heavy tails independently of the channel memory and hence cannot be used to directly determine the memory of the channel.

We now change the prior on each ith element of the measurement noise $n_{b,i}$ and the ijth element of the channel process noise $W_{b,ij}$ from Gaussian to sparse noise sources draw from the Bernoulli-Gaussian distribution. That is,

$$p_{\mathsf{n}_b}(n_{b,i}) = \eta\,\delta(n_{b,i}) + (1-\eta)\,\mathcal{N}\left(n_{b,i}; 0, 1\right), \tag{3.7a}$$

$$p_{\mathsf{W}_b}(W_{b,ij}) = \eta\,\delta(W_{b,ij})\, + (1-\eta)\,\mathcal{N}\left(W_{b,ij}; 0, 1\right), \tag{3.7b}$$

where η is the sparsity rate that we set to 90%. The DMD spectrums for SNR $= -20$ dB and SNR $= 20$ dB with sparse noise sources are shown in Figs. 3.2(a) and 3.2(d) while those of PCA and SVD are depicted in Figs. 3.2(c) and 3.2(f), and 3.2(b) and 3.2(e), respectively. Because sparse noise sources only impact a few components, it becomes possible to distinguish between small and high channel memory at both low and high SNR levels. The DMD spectrums in 3.2(a) and 3.2(d) at low and high SNR levels distinguish the dynamics as a function of the channel memory. The PCA and SVD spectrums, however, are less sensitive to the sparse noise prior, with both low and high

SNR cases being very similar (up to a scaling factor). This confirms again how the focus of PCA (resp. SVD) to encompass the variables with high variations (resp. variables aligned with the eigenmode directions) makes it unable to capture the noise prior and the SNR level.

3.4 Conclusion

This chapter explored the effectiveness of a low-cost method, which is based on the dynamic mode decomposition (DMD), to assess the memory of wireless channels as a function of the signal-to-noise ratio and the noise models. Because DMD is known to be effective in conveying the temporal evolution of dynamical systems, our results confirm that, by using the spectrum of the approximate Koopman operator, the channel memory is also well captured. This is in contrast to PCA which provides limited and non-differentiating information about the channel memory. These results establish DMD as a promising tool for data-driven channel characterization and memory-aware adaptation

Chapter 4

Conclusion and Future Directions

4.1 Concluding Remarks

This thesis addressed two complementary challenges in wireless channel estimation: the need for physically consistent modeling in compact MIMO arrays and the potential of model-free techniques to infer temporal dynamics from observed data.

In the first part, we proposed a Kalman filtering framework that incorporates mutual coupling effects using analytical impedance matrices. By reformulating the channel observation model to account for both self and mutual impedances, the method enables recursive tracking of the physical MIMO channel in a manner that aligns with the underlying electromagnetic behavior. Numerical results showed that the proposed MC-aware estimator consistently outperforms conventional LS and LMMSE approaches, especially in highly correlated and compact array settings.

In the second part, we introduced a data-driven framework for quantifying wireless channel memory using Dynamic Mode Decomposition (DMD). By applying DMD to received signal snapshots over time, we showed that the leading eigenvalue of the Koopman operator provides a meaningful proxy for the channel's temporal correlation level. Unlike PCA and SVD, DMD captures both spatial and temporal dynamics, and operates without requiring pilot signals or explicit model assumptions. The method is particularly suitable for mobility-aware applications in which channel statistics evolve rapidly and adaptivity is critical.

Together, these contributions illustrate the importance of bridging physical modeling with modern data-driven tools to improve wireless channel estimation and characterization in future communication systems.

Future Directions

Several extensions remain open for future work.

- **Receiver Design Based on MC-Aware Estimates:** One possible direction is to incorporate the MC-aware channel estimates into the design of robust receivers. The extended Kalman framework could be adapted to estimate the channel and detect transmitted symbols in an iterative fashion, or to design MMSE receivers that exploit the spatial structure induced by mutual coupling for improved detection performance.

- **Non Constant SNR** While the current study evaluates channel memory at fixed SNR levels, future work could explore scenarios where SNR varies dynamically over time. This would provide insight into the robustness of DMD under fluctuating channel conditions and extend its applicability to real-world fading environments

- **MIMO Extension** A natural extension would be to investigate the effect of varying the number of transmit and receive antennas. Studying the interaction between spatial diversity and temporal memory estimation could uncover new strategies for leveraging MIMO structures in memory-aware system design.

- **Comparison with Other Modal Decompositions:** Although DMD demonstrates superior performance over PCA in capturing channel memory, future studies may compare DMD with other modal decomposition and Machine learning based techniques.

Bibliography

[1] N. Titus and K. P. Extension, "The impact of 5G technology on autonomous vehicles," vol. 3, pp. 36–39, 09 2024.

[2] M. Javaid, A. Haleem, R. P. Singh, and R. Suman, "5G technology for healthcare: Features, serviceable pillars, and applications," *Intelligent Pharmacy*, vol. 1, no. 1, pp. 2–10, 2023.

[3] A. Gohar and G. Nencioni, "The role of 5G technologies in a smart city: The case for intelligent transportation system," *Sustainability*, vol. 13, no. 9, pp. 5188–, 2021.

[4] W. Saad, M. Bennis, and M. Chen, "A vision of 6G wireless systems: Applications, trends, technologies, and open research problems," *IEEE network*, vol. 34, no. 3, pp. 134–142, 2019.

[5] H. Ganame, L. Yingzhuang, H. Ghazzai, and D. Kamissoko, "5G base station deployment perspectives in millimeter wave frequencies using meta-heuristic algorithms," *Electronics*, vol. 8, no. 11, 2019.

[6] M. H. Alsharif, A. H. Kelechi, M. A. Albreem, S. A. Chaudhry, M. S. Zia, and S. Kim, "Sixth generation 6G wireless networks: Vision, research activities, challenges and potential solutions," *Symmetry*, vol. 12, no. 4, p. 676, 2020.

[7] W. Tong and P. Zhu, "6G: The next horizon," in *TITLES*, p. 54, 2022.

[8] A. Ashraf, T. Gunawan, M. Kartiwi, L. Nur, B. Nugroho, and R. Pudji Astuti, "Advancements and challenges in scalable modular antenna arrays for 5G massive MIMO networks," *IEEE Access*, vol. PP, pp. 1–1, 01 2024.

[9] L. J. Chu, "Physical limitations of omni-directional antennas," *Journal of applied physics*, vol. 19, no. 12, pp. 1163–1175, 1948.

[10] R. F. Harrington, "Effect of antenna size on gain, bandwidth, and efficiency[1]," *Journal of Research of the National Bureau of Standards: Radio propagation. D*, vol. 63, 1959.

[11] J. W. Wallace and M. A. Jensen, "Mutual coupling in mimo wireless systems: A rigorous network theory analysis," *IEEE transactions on wireless communications*, vol. 3, no. 4, pp. 1317–1325, 2004.

[12] M. T. Ivrlač and J. A. Nossek, "Toward a circuit theory of communication," *IEEE Transactions on Circuits and Systems I: Regular Papers*, vol. 57, no. 7, pp. 1663–1683, 2010.

[13] A. D. Yaghjian and S. R. Best, "Impedance, bandwidth, and q of antennas," *IEEE Transactions on Antennas and Propagation*, vol. 53, no. 4, pp. 1298–1324, 2005.

[14] S.-H. Xing, C. Zhang, M.-Z. Li, X.-Z. Bo, S.-H. Liu, and Z.-G. Liu, "Simultaneous enhancing decoupling bandwidth and impedance bandwidth of stacked microstrip patch antennas by achieving the mutual coupling nulls," *IEEE Transactions on Antennas and Propagation*, 2025.

[15] M. Akrout, V. Shyianov, F. Bellili, A. Mezghani, and R. W. Heath, "Super-wideband massive MIMO," *IEEE journal on selected areas in communications*, vol. 41, no. 8, pp. 2414–2430, 2023.

[16] Z. Yuanjin, "A novel channel estimation and tracking method for wireless ofdm systems based on pilots and kalman filtering," *IEEE Transactions on Consumer Electronics*, vol. 49, no. 2, pp. 275–283, 2003.

[17] W. Chen and R. Zhang, "Kalman-filter channel estimator for ofdm systems in time and frequency-selective fading environment," in *2004 IEEE International Conference on Acoustics, Speech, and Signal Processing*, vol. 4, pp. iv–iv, IEEE, 2004.

[18] D. C. Dalwadi and H. B. Soni, "A novel channel estimation technique of MIMO-OFDM system based on extended kalman filter," in *2017 4th International Conference on Electronics and Communication Systems (ICECS)*, pp. 158–163, IEEE, 2017.

[19] K. J. Kim, J. Yue, R. A. Iltis, and J. D. Gibson, "A qrd-m/kalman filter-based detection and channel estimation algorithm for MIMO-OFDM systems," *IEEE transactions on wireless communications*, vol. 4, no. 2, pp. 710–721, 2005.

[20] E. Kofidis, "Adaptive joint channel estimation/data detection in flexible multi-carrier MIMO systems—a tensor-based approach," in *ICASSP 2024-2024 IEEE International Conference on Acoustics, Speech and Signal Processing (ICASSP)*, pp. 8721–8725, IEEE, 2024.

[21] C. Ramesh and V. Vaidehi, "Imm based kalman filter for channel estimation in uwb ofdm systems," in *2007 International Conference on Signal Processing, Communications and Networking*, pp. 320–325, IEEE, 2007.

[22] P. De, M. Juntti, and C. K. Thomas, "Multi stage kalman filter (mskf) based time-varying sparse channel estimation with fast convergence," *IEEE Open Journal of Signal Processing*, vol. 3, pp. 21–35, 2021.

[23] M. A. M. Sadr and B. Champagne, "Joint channel estimation and robust beamforming design for af relaying using imm kalman filters," *IEEE Transactions on Vehicular Technology*, vol. 72, no. 2, pp. 1775–1790, 2022.

[24] D. Yu, G. Zheng, A. Shojaeifard, S. Lambotharan, and Y. Liu, "Kalman filter based channel tracking for ris-assisted multi-user networks," *IEEE Transactions on Wireless Communications*, vol. 23, no. 4, pp. 3856–3869, 2023.

[25] R. He, O. Renaudin, V.-M. Kolmonen, K. Haneda, Z. Zhong, B. Ai, and C. Oestges, "A dynamic wideband directional channel model for vehicle-to-vehicle communications," *IEEE Transactions on Industrial Electronics*, vol. 62, no. 12, pp. 7870–7882, 2015.

[26] J. Wu and P. Fan, "A survey on high mobility wireless communications: Challenges, opportunities and solutions," *IEEE Access*, vol. 4, pp. 450–476, 2016.

[27] C.-p. Li and M. J. Neely, "Exploiting channel memory for multiuser wireless scheduling without channel measurement: Capacity regions and algorithms," *Performance Evaluation*, vol. 68, no. 8, pp. 631–657, 2011.

[28] S. Coleri, M. Ergen, A. Puri, and A. Bahai, "Channel estimation techniques based on pilot arrangement in ofdm systems," *IEEE Transactions on broadcasting*, vol. 48, no. 3, pp. 223–229, 2002.

[29] Z. Du, X. Song, J. Cheng, and N. C. Beaulieu, "Maximum likelihood based channel estimation for macrocellular ofdm uplinks in dispersive time-varying channels," *IEEE Transactions on Wireless Communications*, vol. 10, no. 1, pp. 176–187, 2010.

[30] J. Ma, S. Zhang, H. Li, N. Zhao, and A. Nallanathan, "Iterative lmmse individual channel estimation over relay networks with multiple antennas," *IEEE Transactions on Vehicular Technology*, vol. 67, no. 1, pp. 423–435, 2017.

[31] L. Wang, G. Liu, J. Xue, and K.-K. Wong, "Channel prediction using ordinary differential equations for MIMO systems," *IEEE Transactions on Vehicular Technology*, vol. 72, no. 2, pp. 2111–2119, 2022.

[32] W. Jiang and H. D. Schotten, "Neural network-based fading channel prediction: A comprehensive overview," *IEEE Access*, vol. 7, pp. 118112–118124, 2019.

[33] E. Karami, "Tracking performance of least squares MIMO channel estimation algorithm," *IEEE Transactions on Communications*, vol. 55, no. 11, pp. 2201–2209, 2007.

[34] C. Wu, X. Yi, Y. Zhu, W. Wang, L. You, and X. Gao, "Channel prediction in high-mobility massive MIMO: From spatio-temporal autoregression to deep learning," *IEEE Journal on Selected Areas in Communications*, vol. 39, no. 7, pp. 1915–1930, 2021.

[35] E. Nayebi and B. D. Rao, "Semi-blind channel estimation for multiuser massive MIMO systems," *IEEE Transactions on Signal Processing*, vol. 66, no. 2, pp. 540–553, 2017.

[36] T. Peken, G. Vanhoy, and T. Bose, "Blind channel estimation for massive MIMO," *Analog Integrated Circuits and Signal Processing*, vol. 91, pp. 257–266, 2017.

[37] C. Huang, A. F. Molisch, R. He, R. Wang, P. Tang, and Z. Zhong, "Machine-learning-based data processing techniques for vehicle-to-vehicle channel modeling," *IEEE Communications Magazine*, vol. 57, no. 11, pp. 109–115, 2019.

[38] J. N. Kutz, S. L. Brunton, B. W. Brunton, and J. L. Proctor, *Dynamic mode decomposition: data-driven modeling of complex systems*. SIAM, 2016.

[39] A. Muniraju, "Analysis of dynamic mode decomposition," Master's thesis, The University of Wisconsin-Milwaukee, 2018.

[40] J. H. Tu, *Dynamic mode decomposition: Theory and applications.* PhD thesis, Princeton University, 2013.

[41] A. H. Jazwinski, *Stochastic Processes and Filtering Theory.* Academic Press, 1970.

[42] T. Kailath, A. H. Sayed, and B. Hassibi, *Linear Estimation.* Prentice Hall, 2000.

[43] M. Akrout, A. Feriani, F. Bellili, A. Mezghani, and E. Hossain, "Continual learning-based mimo channel estimation: A benchmarking study," in *ICC 2023-IEEE International Conference on Communications*, pp. 2631–2636, IEEE, 2023.

[44] W. C. Jakes and D. C. Cox, *Microwave mobile communications.* Wiley-IEEE press, 1994.

Appendix A

Impedance-Based MIMO Modeling

This appendix provides the derivation of the impedance-based model for mutual coupling in multi-antenna systems, based on network theory.

A.1 Impedance-Based MIMO Model

We represent a multi-port network system, where the transmit and receive antenna arrays experience mutual coupling. The impedance matrix is given by:

$$\begin{bmatrix} \boldsymbol{v}_T \\ \boldsymbol{v}_R \end{bmatrix} = \begin{bmatrix} \boldsymbol{Z}_T & \boldsymbol{Z}_{TR} \\ \boldsymbol{Z}_{RT} & \boldsymbol{Z}_R \end{bmatrix} \begin{bmatrix} \boldsymbol{i}_T \\ \boldsymbol{i}_R \end{bmatrix}. \tag{A.1}$$

$$\boldsymbol{v}_T = \boldsymbol{Z}_T \boldsymbol{i}_T + \boldsymbol{Z}_{TR} \boldsymbol{i}_R. \tag{A.2}$$

$$\boldsymbol{v}_R = \boldsymbol{Z}_R \boldsymbol{i}_R + \boldsymbol{Z}_{RT} \boldsymbol{i}_T. \tag{A.3}$$

Applying Kirchhoff's Voltage Law (KVL) at the receiver:

$$\boldsymbol{v}_R = -\tilde{\boldsymbol{v}}_{N,R} - R_{\text{in}} \boldsymbol{i}_R. \tag{A.4}$$

$$\boldsymbol{Z}_R \boldsymbol{i}_R + \boldsymbol{Z}_{RT} \boldsymbol{i}_T = -\tilde{\boldsymbol{v}}_{N,R} - R_{\text{in}} \boldsymbol{i}_R. \tag{A.5}$$

Solving for $\boldsymbol{i}_R$:

$$\boldsymbol{i}_R = -(\boldsymbol{Z}_R + R_{\text{in}}\boldsymbol{I}_M)^{-1}(\tilde{\boldsymbol{v}}_{N,R} + \boldsymbol{Z}_{RT}\boldsymbol{i}_T). \tag{A.6}$$

Define:

$$\boldsymbol{T} = (\boldsymbol{Z}_R + R_{\text{in}}\boldsymbol{I}_M)^{-1}, \tag{A.7}$$

Then:

$$\boldsymbol{i}_R = -\boldsymbol{T}(\tilde{\boldsymbol{v}}_{N,R} + \boldsymbol{Z}_{RT}\boldsymbol{i}_T). \tag{A.8}$$

The transmit current is:

$$\boldsymbol{i}_T = \left(\boldsymbol{Z}_T + R\boldsymbol{I}_N - \boldsymbol{Z}_{TR}\boldsymbol{T}\boldsymbol{Z}_{RT}\right)^{-1}\left(\boldsymbol{v}_G - \tilde{\boldsymbol{v}}_{N,R} + \boldsymbol{Z}_{TR}\boldsymbol{T}\tilde{\boldsymbol{v}}_{N,R}\right). \tag{A.9}$$

Under far-field approximation:

$$\boldsymbol{S} = (\boldsymbol{Z}_T + R\boldsymbol{I}_N)^{-1}. \tag{A.10}$$